

# Degenerate Mode Birdcage Volume Coil for Sensitivity-Encoded Imaging

Fa-Hsuan Lin,<sup>1–3</sup> Kenneth K. Kwong,<sup>2,3</sup> Ing-Jye Huang,<sup>3,4</sup> John W. Belliveau,<sup>2,3</sup> and Lawrence L. Wald<sup>2,3\*</sup>

**A volume birdcage coil for accelerated image encoding with parallel acquisition methods such as SENSE is demonstrated. The coil is degenerately tuned with both the standard homogeneous mode and the first gradient mode of the birdcage coil resonant at the Larmor frequency. Conventional and antisymmetric coupling structures allow imaging from each of these modes simultaneously. The coil for SENSE-type reconstruction with acceleration factors of up to 2-fold is demonstrated. The spatial distribution of the added noise from the SENSE reconstruction (g-factor map) due to geometrical arrangement of the two-channel system is estimated. The spatially averaged g-factors were found to be 1.21, 1.36, and 1.55 for 1.3, 1.6, and 2-fold accelerations, respectively. The system was demonstrated in vivo using accelerated and nonaccelerated anatomical brain images at 1.5 T. The maximal 2-fold acceleration in this dual-mode degenerate birdcage coil offers the potential to extend SENSE-type image reconstruction methods to applications demanding uniform whole brain coverage. Magn Reson Med 50:1107–1111, 2003. © 2003 Wiley-Liss, Inc.**

**Key words:** parallel MRI; SENSE; birdcage; RF coil; brain

Although first proposed for increasing sensitivity and spatial coverage, simultaneous imaging from multiple surface coils has recently seen widespread use as a way of decreasing image encoding times utilizing either SENSE-based or SMASH-based techniques (1,2). These methods rely on the differing spatial profiles of the array elements to reconstruct the undersampled image. Successful reconstruction favors spatially differing sensitivity profiles such as those derived from a nonoverlapping (gapped) array of surface coils (1–3). The surface coil array, especially those utilizing smaller surface coil elements, necessarily have a sensitivity profile which decreases with depth into the tissue. Clinical applications, however, often favor the homogeneous coverage of the birdcage coil. For this reason, volume birdcage head coils have become the standard for clinical brain imaging. Because of its excellent homogeneity and simple spatial relationship of its two orthogonal homogeneous modes, the uniform birdcage mode alone does not provide the additional spatial information

<sup>1</sup>Harvard-MIT Division of Health Sciences and Technology, Boston, Massachusetts.

<sup>2</sup>Department of Radiology, Massachusetts General Hospital, Boston, Massachusetts.

<sup>3</sup>MGH-HMS-MIT Athinoula A. Martinos Center for Biomedical Imaging, Charlestown, Massachusetts.

<sup>4</sup>Department of Electrical Engineering, National Taiwan University, Taipei, Taiwan.

\*Correspondence to: Lawrence L. Wald, A. A. Martinos Center for Biomedical Imaging, Bldg. 149 13th Street, Mailcode 149-2301, Charlestown, MA 02129. E-mail: wald@nmr.mgh.harvard.edu

Received 3 March 2003; revised 27 June 2003; accepted 15 July 2003.

DOI 10.1002/mrm.10632

Published online in Wiley InterScience (www.interscience.wiley.com).

© 2003 Wiley-Liss, Inc.

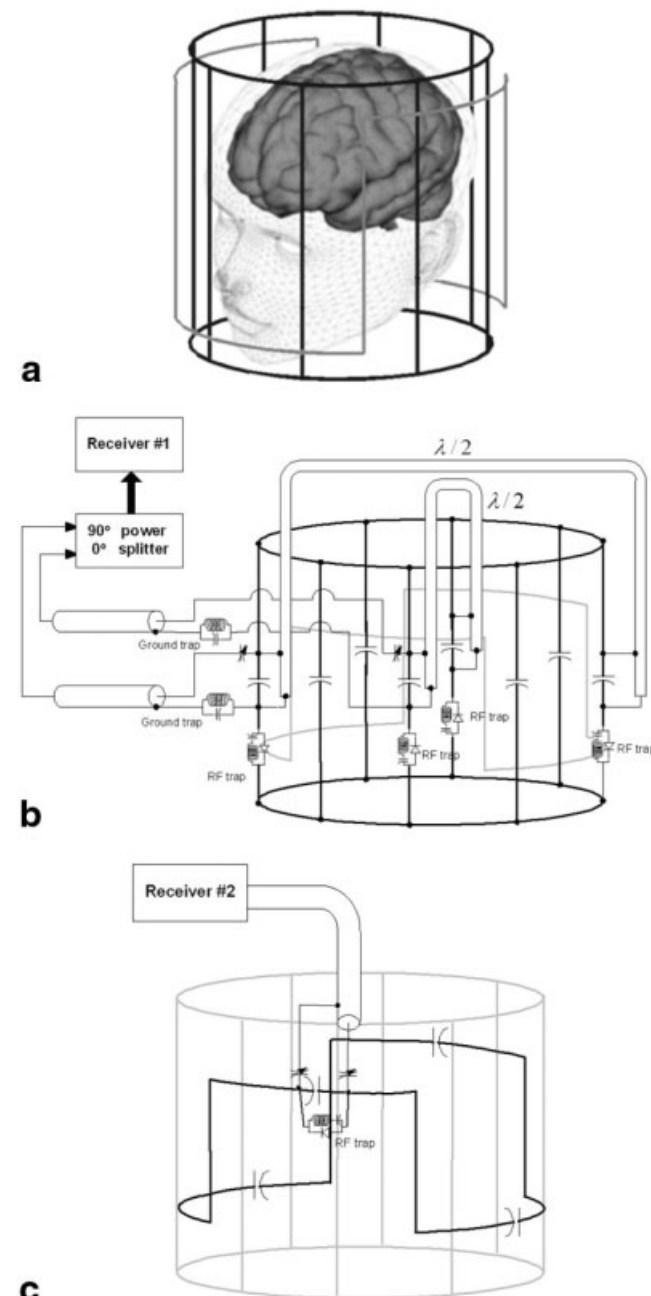


**FIG. 1.** **a:** The geometry of the dual-mode degenerate birdcage. **b:** The coupling circuit for the coil. **c:** Detail of the antisymmetric coupling structure to pull the frequency of the gradient mode to the Larmor frequency and to selectively couple to the gradient mode.

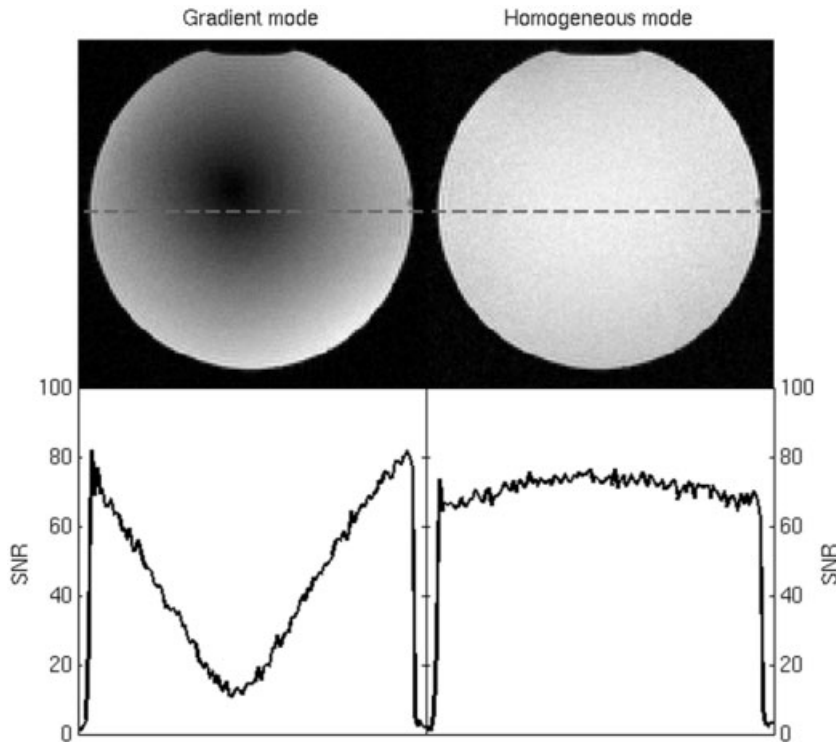


FIG. 2. Phantom images from homogenous mode (right) and gradient mode (left). SNR plots from the cross section depicted by the gray dashed line.

needed for SENSE reconstruction. The higher-order modes of the birdcage, however, have substantially differing spatial magnitude profiles from the uniform mode, and all of the modes differ from one another in phase profiles. In this case, the benefits of parallel imaging encoding acceleration schemes can be achieved while preserving uniform image acquisition.

Detection of the MR signal from degenerate modes of the birdcage coil has been explored for both SNR enhancement (4,5) and for decreased image encoding times (6). In order to evaluate the potential for SENSE acceleration with uniform signal detection, we utilize a degenerate mode birdcage in which the homogeneous and gradient modes of the coil are simultaneously detected. The two homogeneous modes are combined in quadrature and detected in receiver 1, and the first gradient mode of the birdcage structure is also tuned to the Larmor frequency and detected in receiver 2. The spatially differing nature of the two modes makes them well suited to a maximum of 2-fold acceleration with the SENSE method. The uniform nature of the homogeneous mode provides image uniformity nearing that of traditional birdcage coils.

## MATERIALS AND METHODS

An eight-rung low-pass quadrature birdcage volume coil (26.3 cm diameter and 33.5 cm length) tuned for a 1.5 T scanner (Siemens Symphony Sonata, Siemens Medical Solutions, Iselin, NJ) was constructed for this study. The birdcage was used in the “receive-only” mode. The body coil was used for uniform excitation. The homogeneous (lowest frequency) mode of the low-pass birdcage was connected to the first receiver using a four-port (0°, 90°, 180°, 270°) drive with conventional capacitive coupling.

The 0°, 90°, 180°, and 270° legs were combined with a conventional 90° hybrid coupler driving two rungs 90° apart, in conjunction with two  $\lambda/2$  RG-58 coaxial cables connecting opposite rungs of the driving legs, as shown in Fig. 1b. This 4-port drive is necessary to ensure that only the uniform mode is coupled into the first receiver. The next highest mode of the birdcage (a gradient mode) shows a high sensitivity at the periphery of the coil and a decreasing sensitivity profile near the center of the birdcage. Ideally, there is no  $B_1$  field at the center of the coil. In addition to the linear change in  $B_1$  magnitude across the diameter, opposite sides of the coil have a  $B_1$  field phase difference of 180°. Since the 2nd (gradient) mode of the conventional low-pass birdcage resonates at a higher frequency than the uniform mode, it is necessary to selectively perturb the frequency of this mode to make it resonant at the Larmor frequency. For the coil geometry used, the gradient mode resonated at a frequency 11.5 MHz above the uniform mode. In this work, we tuned the gradient mode to the Larmor frequency using a resonant antisymmetric coupling structure around the coil whose symmetry allows

Table 1

G-factors of the Accelerated SENSE Acquisitions at 1.33 (75% of full PE), 1.60 (62.5% of full PE), and 2.0 (50% of full PE)

SENSE acceleration	Median	Average	SD	Max	Min
1.33 (75%)	1.00	1.21	0.87	40.32	1.00
1.60 (62.5%)	1.09	1.36	1.53	160.51	1.00
2.00 (50%)	1.29	1.55	1.46	87.68	1.00

In the table, acceleration is the reciprocal of the ratio between the number of phase encoding line in SENSE acquisition and full FOV acquisition.

coupling only to the gradient mode (4). This antisymmetric coupling structure has a zigzag anti-Helmholtz configuration shown in Fig. 1c. Although not resonant at the Larmor frequency, adjusting the resonant frequency of the antisymmetric coupling structure allows it to be used to pull the gradient mode of the birdcage to a lower frequency. Its antisymmetric symmetry does not allow it to perturb the resonance frequency of the homogeneous mode. The signal coupled out of the antisymmetric structure via capacitive coupling was connected to the second receiver. The configuration of the dual-mode birdcage volume coil is illustrated in Fig. 1. Active pin diode traps were placed on every other rung to actively detune the birdcage structure during RF transmission using the body coil. An active RF trap was also mounted on the gradient mode antisymmetric coupling structure to avoid the coupling between body coil and this structure during RF transmission. Additionally, four passive RF cable traps were placed where the coaxial cables connected to the coil to block common-mode currents on the cables.

The birdcage coil was tested on the bench using a network analyzer (Hewlett-Packard model 4395A, Palo Alto, CA).  $S_{11}$  parameters were measured for both the homogeneous mode and gradient mode separately to ensure sufficient tuning and matching. Coil tuning and identification of the modes was also performed using  $S_{12}$  measures and appropriate shielded inductive probes. Isolation between the homogeneous and gradient modes was measured with an  $S_{12}$  measure between the two modes.

To test the coil performance and noise amplification during SENSE acquisition, phantom images were acquired using a gradient echo sequence (TR/TE/flip = 100 ms / 5.4 ms / 90°, FOV = 170 × 170 mm; slice thickness = 5 mm; image matrix = 256 × 256). In addition to the full phase-encoded images (100% phase encoding (PE), 256 PE lines), we acquired aliased images of 75% (192 PE lines), 62.5% (160 PE lines), and 50% (128 PE lines) of full 256 phase-encoding steps. Unfolding of the images to full FOV were reconstructed by in vivo sensitivity reconstruction (7). Specifically, this is formulated by the following linear equation:

$$\tilde{y} = A \times \bar{x}. \quad [1]$$

$\tilde{y}$  is the undersampled data from the array coil,  $\bar{x}$  denotes the unknown spin density, and  $A$  is the encoding matrix representing the undersampling (3). Noise amplification from parallel MRI was estimated by the g-factor (2):

$$g_p = \sqrt{[(A^H \Psi A)^{-1}]_{p,p} (A^H \Psi A)_{p,p}} \quad [2]$$

where  $A$  is the encoding matrix;  $\Psi$  is the noise covariance matrix; and  $A^H$  denotes Hermitian operation. The noise covariance matrix was assumed to be diagonal (noise uncorrelated between the receivers). Noise levels were estimated from the signal variance in the airspace outside the head in raw complex images. The SNR of each mode was measured by region of interest measurement from the magnitude image produced by each receiver. The spatial profile of the reception field of each mode was visualized by plotting a line through the center of the phantom.

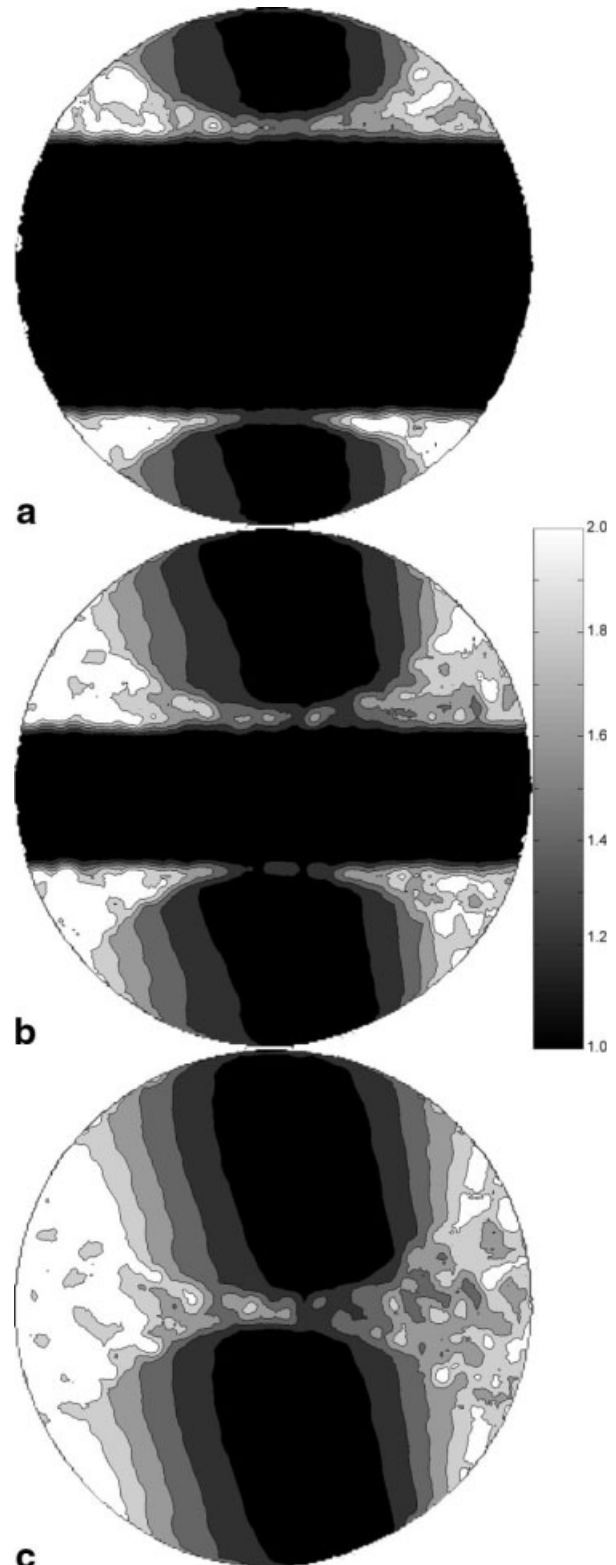


FIG. 3. The noise amplification due to geometrical arrangement of the array coil (g-factor map). **a:** The g-factor map of 1.33-fold acceleration (75% phase encoding). **b:** The g-factor map of 1.60-fold acceleration (62.5% phase encoding). **c:** The g-factor map of 2.00-fold acceleration (50% phase encoding). In these figures, g-factors higher than 2.0 were thresholded to 2.0 for better illustration of the spatial distribution of the g-factor maps.

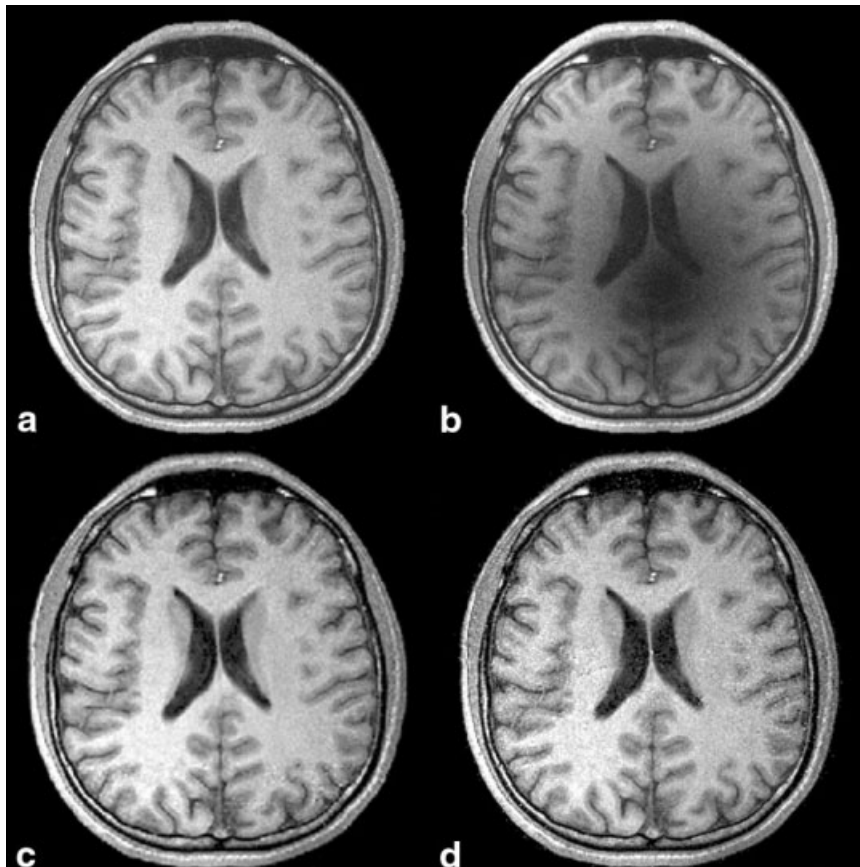


FIG. 4. In vivo brain magnitude images from the quadrature homogeneous mode (a) and the gradient mode (b) in full-FOV reference scan. The reconstructed image from 1.3- and 2.0-fold accelerated SENSE acquisition is shown in c and d, respectively.

In vivo anatomical images were also collected from a healthy subject using the same 1.5 T scanner using slab-excitation 3D FLASH sequence after approval by the Institutional Review Board and informed consent. The imaging parameters for anatomical images were TR/TE/flip = 20 ms / 4 ms / 27°, FOV = 200 mm \* 200 mm \* 144 mm; slice thickness = 3.0 mm; 48 partitions; image matrix = 256 (x) \* 256 (y) \* 48 (z). In addition to the full phase-encoded images (100% PE, 256 PE lines), we acquired aliased images of 75% (192 PE lines), 62.5% (160 PE lines), and 50% (128 PE lines) of full 256 PE steps. To assess the uniformity in the reconstructed images, we computed the standard deviation (SD) as a percent of the mean value within the white matter region defined by manual segmentation.

## RESULT

Prior to connecting the zig-zag structure to collapse the gradient mode and the homogeneous mode, the splitting of the two modes was found to be 11.5 MHz. By starting with the tuning of the zig-zag structure far below resonance and adjusting its capacitance, the gradient mode can be steadily adjusted down in frequency until it superimposes on the uniform mode.

The  $S_{12}$  parameter was measured between the gradient mode and the combined quadrature homogeneous modes of the coil. The isolation on the bench without loading was 30 dB, which decreased to 23 dB when loaded with a spherical saline phantom of 25 cm diameter. Figure 2

shows the individual phantom images from the homogeneous mode and gradient mode as detected by the two independent receivers. Qualitatively, the phantom magnitude image of the homogeneous mode gives a relatively constant reception across the FOV. The gradient mode, however, shows the predicated sensitivity field pattern—almost null reception sensitivity at the center of the coil and high sensitivity near the periphery of the coil.

The phantom SNR of the homogeneous mode of the quadrature-driven birdcage was found to be 68 with an SD of 3 across the FOV. The gradient mode produced a maximum SNR of 84 at the edges of the phantom and a minimum SNR of 0.2 near the center. The lower panel of Fig. 2 shows the SNR plotted for each mode for the central line of pixels in a transverse slice through the phantom. For this line, the homogeneous mode has maximal SNR of 76 and minimal SNR of 62 (average 71, SD 3), while gradient mode has maximal SNR of 82 and minimal SNR of 10 (average 44, SD 22).

The noise amplification in the SENSE acquisition due to the geometrical arrangement of the array coil was assessed using Eq. [2]. The measured g-factors are listed in Table 1. As expected, the median and average g-factors increase when the acceleration factor increases. Figure 3 shows the g-factor maps for three accelerated acquisitions listed in Table 1.

Figure 4 shows an axial slice from a normal volunteer for the full FOV acquisition and SENSE reconstruction using 1.33-fold acceleration (PE = 75%) and 2.0-fold acceleration (PE = 50%). The top panel shows the two anatomical

images from the homogeneous and gradient channel separately. The center of the brain had significant reduced signal in the gradient mode image. The SD across white matter in the brain slice was 19.2% of the mean for the homogeneous mode in the full FOV reference image. The SDs of the white matter pixel intensity in the 1.33-fold and 2.0-fold SENSE reconstructions were found to be 20.6% and 21.0% of the mean.

## DISCUSSION

In this study, the uniform and first gradient mode of a birdcage coil are simultaneously detected to enable SENSE acceleration with a traditional birdcage structure. The homogeneous mode, which gives uniform FOV coverage, and the gradient mode, with its spatially varying  $B_1$  field, provide independent views, which can be used for the SENSE reconstruction. Since the maximum acceleration factor is determined by the number of independent receivers (usually the number of elements in the array), the dual mode birdcage coil is limited to 2-fold SENSE/SMASH acceleration. For an  $n$  rung birdcage there exists  $n/2 + 1$  modes, which could in principle be detected and utilized for increased SENSE accelerations. The higher-order modes, however, tend to be similar to the gradient mode in magnitude, but their more complicated spatial distributions of  $B_1$  phase might be useful for SENSE reconstruction. Like the structure demonstrated here to selectively couple into the first gradient mode, dedicated coupling structures that exploit the phase relationship of the higher modes might prove workable.

The aliased airspace region in the calculated g-factor maps was found to have a significantly higher g-factor than other areas within the image. This is typical for SENSE reconstruction and results from the ill-conditioned matrix inversion when a low signal airspace region is aliased with the brain. The areas with increased g-factor could also be further improved by conditioning the inversion process (7) to decrease the noise amplification in SENSE.

Most coils developed for brain imaging with SENSE reconstruction have utilized traditional overlapped surface coil arrays or gapped surface coil elements. For example, an optimized 8-channel gapped phase array for brain SENSE (8) showed good sensitivity and better g-factor performance than the birdcage demonstrated here, but the

uneven spatial SNR distribution may be problematic for clinical applications. The inhomogeneous surface coil image intensity profile may be corrected during or after the SENSE reconstruction (9–12). However, the SNR variations across the head are not compensated using this approach. In this work we demonstrate an approach for clinical imaging which allows modest SENSE acceleration factors while preserving the uniform detection efficiency required by many clinical imaging applications.

## ACKNOWLEDGMENTS

This work was supported in part by The National Center for Research Resources (P41RR14075) and the Mental Illness and Neuroscience Discovery (MIND) Institute.

## REFERENCES

1. Sodickson DK, Manning WJ. Simultaneous acquisition of spatial harmonics (SMASH): fast imaging with radiofrequency coil arrays. *Magn Reson Med* 1997;38:591–603.
2. Pruessmann KP, Weiger M, Scheidegger MB, Boesiger P. SENSE: sensitivity encoding for fast MRI. *Magn Reson Med* 1999;42:952–962.
3. Sodickson DK, McKenzie CA. A generalized approach to parallel magnetic resonance imaging. *Med Phys* 2001;28:1629–1643.
4. Wong EC, Luh W-M. A multimode, single frequency birdcage coil for high sensitivity multichannel whole volume imaging. In: Proc 7th Scientific Meeting ISMRM, Philadelphia, 1999.
5. Leussler C, Stimma J, Roeschmann P. The bandpass birdcage resonator modified as a coil array for simultaneous MR acquisition. In: Proc 5th Scientific Meeting ISMRM, Vancouver, 1997.
6. Carlson JW, Minemura T. Imaging time reduction through multiple receiver coil data acquisition and image reconstruction. *Magn Reson Med* 1993;29:681–687.
7. Sodickson DK. Tailored SMASH image reconstructions for robust in vivo parallel MR imaging. *Magn Reson Med* 2000;44:243–251.
8. de Zwart JA, Ledden PJ, Kellman P, van Gelderen P, Duyn JH. Design of a SENSE-optimized high-sensitivity MRI receive coil for brain imaging. *Magn Reson Med* 2002;47:1218–1227.
9. Wald LL, Carvajal L, Moyher SE, Nelson SJ, Grant PE, Barkovich AJ, Vigneron DB. Phased array detectors and an automated intensity-correction algorithm for high-resolution MR imaging of the human brain. *Magn Reson Med* 1995;34:433–439.
10. Maurer Jr CR, Aboutanos GB, Dawant BM, Gadamsetty S, Margolin RA, Maciunas RJ, Fitzpatrick JM. Effect of geometrical distortion correction in MR on image registration accuracy. *J Comput Assist Tomogr* 1996; 20:666–679.
11. Cohen MS, DuBois RM, Zeineh MM. Rapid and effective correction of RF inhomogeneity for high field magnetic resonance imaging. *Hum Brain Mapp* 2000;10:204–211.
12. Lin F-H, Chen Y-J, Belliveau JW, Wald LL. A wavelet-based approximation of surface coil sensitivity profiles for correction of image intensity inhomogeneity and parallel imaging reconstruction. *Hum Brain Mapp* 2003;19:96–111.